OCEANOGRAPHIC AND ATMOSPHERIC RETRIEVALS FROM AVIRIS HYPERSPECTRAL DATA

Craig Gelpi, Benjamin C. Schuraytz, and Matthew E. Husman[1]

1. INTRODUCTION

The ocean and coastal zone are particularly challenging environments for using high-altitude, hyperspectral data. To discern ocean characteristics, atmospheric effects must be compensated for; not only does absorption by atmospheric gases affect a large portion of the reflective spectrum, but atmospheric path scattering contributes a much greater percentage of the measured radiance than that which emanates from the surface and water column. Additionally, the water surface has a strong bi-reflectance distribution function (BRDF) that changes as a function of wind and wave conditions. These effects, too, must be compensated for to make full use of hyperspectral signatures of water column and surface phenomena, an area rich in potential for hyperspectral applications.

We are developing hyperspectral techniques to perform these compensations for over-ocean analysis. One method, the Modulated Surface Reflectance (MSR) algorithm (Gelpi, 2000; Gelpi and Nguyen, 2000), employs scale-size differences between atmospheric variations and the modulated radiance produced by surface waves to remove atmospheric path-scattered radiance. The modulated-radiance spectrum is used directly to compute water-vapor column density, which is required to compensate for water-vapor absorption. In the present work, we continue to exploit the modulated radiance by developing techniques that relate its amplitude to the surface waveheight by accounting for atmospheric and surface effects. Although waveheight is a desired quantity in its own right, these techniques promise to be especially useful for the analysis of hyperspectral data gathered from satellites, where sea and atmospheric conditions are expected to be inhomogeneous across the image.

In the following sections we give the modulation transfer function relating waveheight to at-sensor radiance modulations and sketch its derivation. Then we retrieve atmospheric and oceanic parameters required to compute the waveheight spectrum, perform the calculation and compare the resulting spectrum to measurements made by nearby NOAA (National Oceanic and Atmospheric Administration) buoys. Retrieved atmospheric parameters are compared to radiative transfer calculations executed with MODTRAN to estimate aerosol characteristics. Finally we remove atmospheric and ocean surface reflectance effects from the at-sensor radiance to derive upwelling, water-column radiance.

[1] XonTech, Inc., 6862 Hayvenhurst Ave., Van Nuys, California 91406, USA
craig_gelpi@xontech.com

2. MODULATION TRANSFER FUNCTION

We develop a modulation transfer function applicable to geometries where sun glint is the most significant factor in the surface reflectance. Cox and Munk (1954) derived the relationship between the received radiance and the ocean wave statistics. Using a Gaussian distribution for the wave slopes, they computed the expected radiance reflected into the sensor. We modify their model to include waves resolved by the sensor's spatial sampling. In our model the large-scale, resolved waves are deterministic while the small-scale waves are described by Gaussian statistics. The at-sensor radiance, spatial power spectral density, P_L, is related to the large-scale waveheight spectrum, P, via the modulation transfer function, M, *i.e.*,

$$P_L\left(\vec{k}\right) = M\left(\vec{k}\right)P\left(\vec{k}\right). \tag{1}$$

To second order in the large-scale to small-scale wave slope ratio, and for observations that do not include the "hot spot", the transfer function is given by

$$M\left(\vec{k}\right) = \left[\frac{E_0(\lambda)\left(1+\left|\nabla\zeta\right|^2\right)^2}{2\pi\cos\theta}\frac{T\rho_{sp}(\chi)}{\sigma^4}e^{-\frac{(\nabla\zeta)^2}{\sigma^2}}\nabla\zeta\cdot\vec{k}\right]^2 \tag{2}$$

where

E_0 solar irradiance at top of the atmosphere.
λ electromagnetic wavelength.
$\nabla\zeta$ surface slope required for specular reflection.
T two-way atmospheric transmittance.
ρ_{sp} Fresnel reflectivity of water surface.
σ^2 small-scale wave slope variance.
$\vec{k}$ spatial wavevector.
θ view angle from nadir.
χ incidence angle.

In addition to the observation geometry, the transfer function depends on the environmental parameters T, σ^2, and ρ_{sp}. Note that M vanishes for waves that propagate perpendicularly to the required slope. These waves are invisible to the sensor. M also is zero where the required slope is zero, *i.e.*, at the "hot spot". This condition is not present in the data analyzed below.

3. DATA SETS AND ATMOSPHERIC AND OCEANIC PARAMETERS

Computing the waveheight from the radiance requires the atmospheric transmittance, small-scale wave slope variance, and the Fresnel reflectivity. In the absence of surfactants we assume the surface reflectivity is that corresponding to the air-seawater interface. When environmental

conditions are homogeneous, we can take advantage of AVIRIS's large field of view (>30^{o}) to derive the other environmental parameters by using the BRDF of the ocean to relate the change in at-sensor radiance to view angle.

We searched the AVIRIS archives for recent over-ocean campaigns where apparent homogeneous atmospheric conditions were encountered and the flight trajectory was linear. We found 2 flights: f970410t01p02r02 and f970414t01p02r02, executed on April 10 and 14, 1997, respectively, over the Santa Barbara Channel of California. Conditions in the Channel are measured with NOAA buoys; the significant wave height (SWH) was 2.9 m and 2.2 m at the westernmost buoy for April 10th and 14th, respectively. An example of the April 10th data is shown in Figure 1. Waves are clearly visible and there are apparent white caps, consistent with the large SWH.

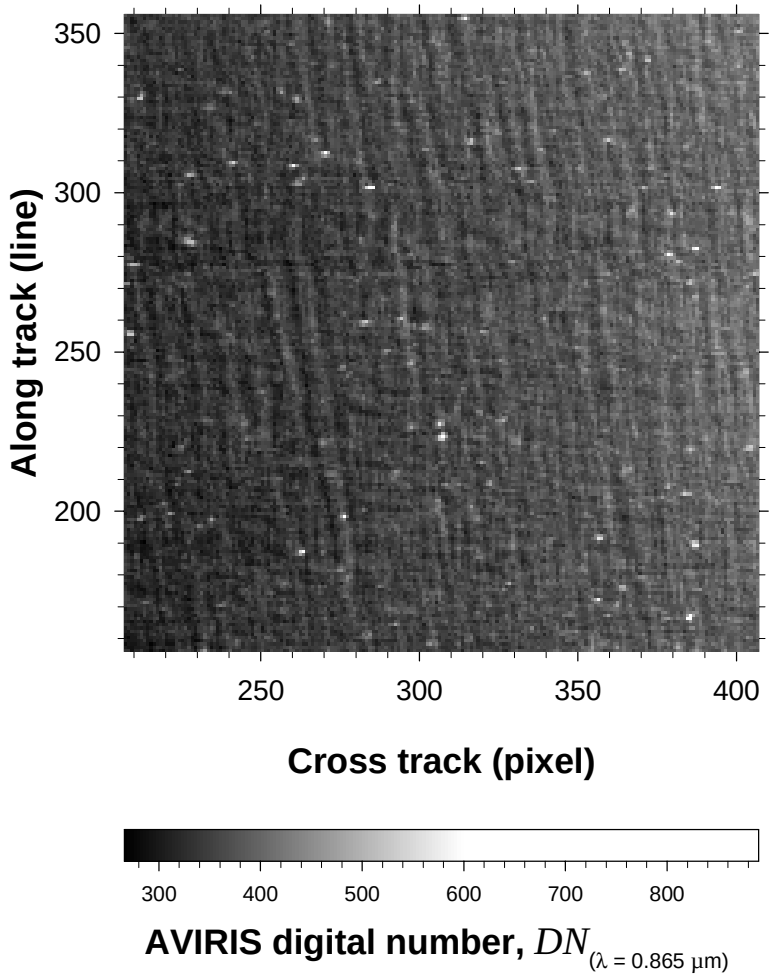

Figure 1. Raw data image of band 54 excised from scene 4 of AVIRIS flight f970410t01p02r02.

For infrared bands (those that exhibit no upwelling, water-column radiance) the line (along-track) ensemble radiance, L^s, should satisfy

$$\left\langle L^s(\lambda,\theta)\right\rangle = \frac{E_0(\lambda)\left(1+\left|\nabla\zeta(\theta)\right|^2\right)^2}{4\pi\cos\theta}\frac{T\rho_{sp}(\chi)}{\sigma_t^2}e^{-\frac{(\nabla\zeta)^2}{\sigma^2}} + \frac{L^P(\lambda)}{\cos\theta}. \tag{3}$$

We have included contributions from the path radiance, L^p but have ignored the scattering phase function. Equation 3 also uses the total slope variance, σ_t^2. The ensemble removes the effects of small-scale waves.

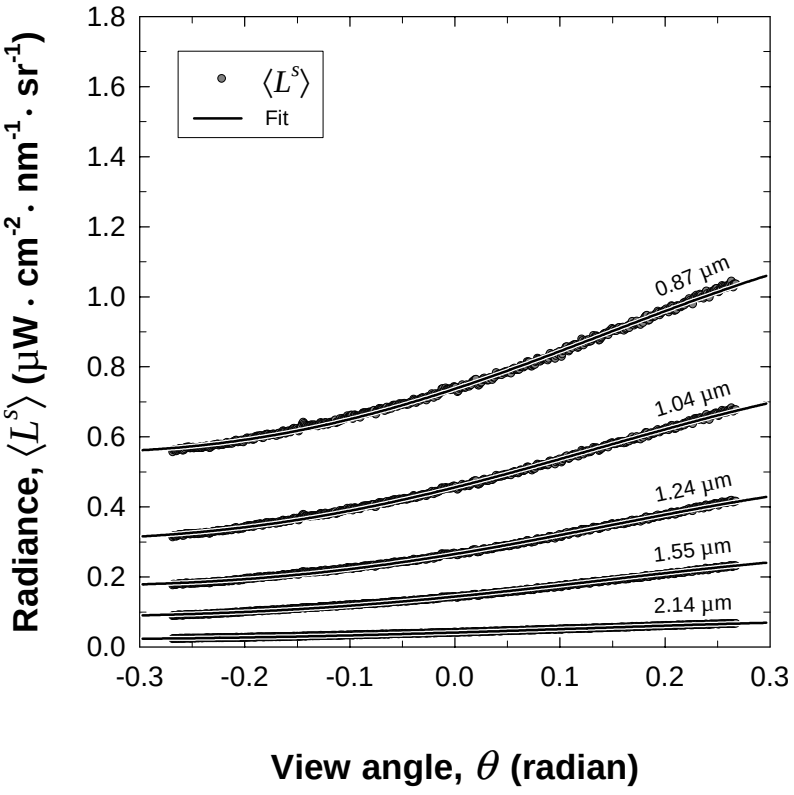

Figure 2. Line ensembles and fits for data from scene 4 of AVIRIS flight f970410t01p02r02.

We fit the total-slope variance, transmittance, and path radiance in the above equation to the ensemble. The data and the goodness of the fit for the April 10th case at several wavelengths are shown in Figure 2. The fitted values for the transmittance and wave slope variance are shown as a function of wavelength in Figure 3. In this case the total wave slope variance is 0.06. Using

buoy data to estimate that portion of the total wave-slope variance produced by the large waves, we can estimate the variance of the small-scale wave slopes.

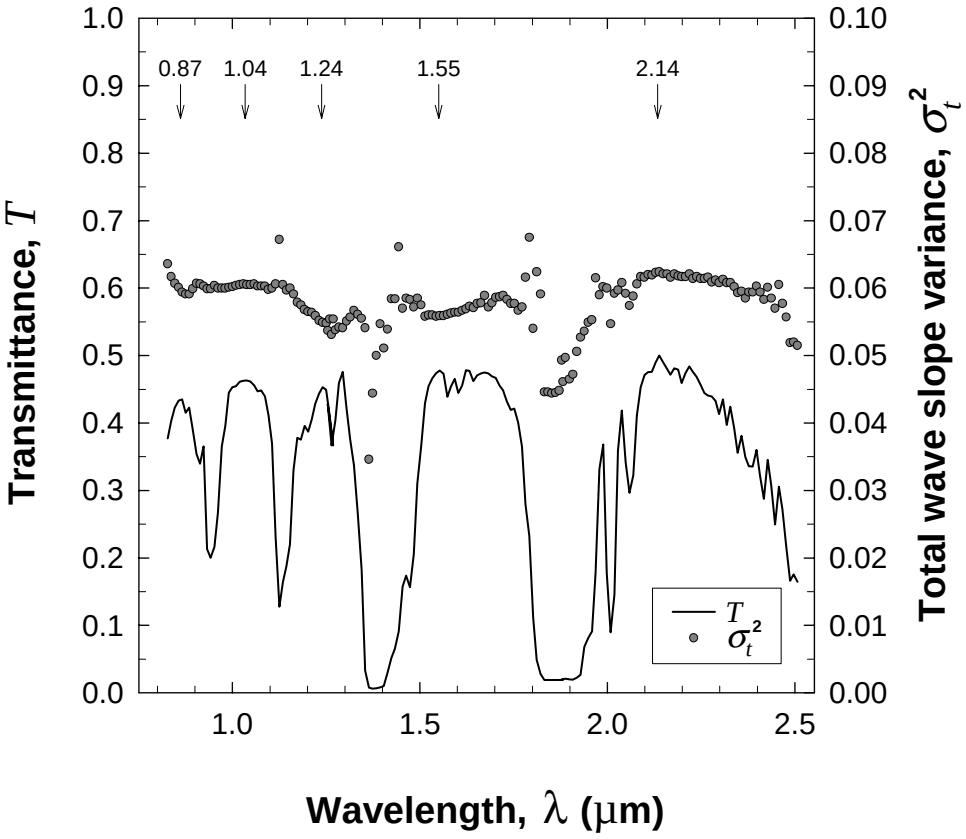

Figure 3. Fitted transmittance and total wave slope variance retrievals from scene 4 of AVIRIS flight f970410t01p02r02.

The fitted transmittance was unexpectedly low for the April 10th data. However, we were able to construct a reasonable aerosol model that closely reproduced both the fitted transmittance and path radiance when employed in the radiative transfer calculations embodied in MODTRAN. We used a 70% standard maritime component that is used in ATREM and a 30% custom urban model. Our custom model employed the standard dust-like and water-soluble parts supplied by ATREM, but we added a soot component that is lognormal with a mean radius of 0.1 μm and with a standard deviation of 2.50 μm. Loading was chosen to give a visibility of 18 km. Water vapor amounts were chosen to be consistent those found with our MSR algorithm. The fitted and modeled spectra for the transmittance and path radiance are compared in Figure 4.

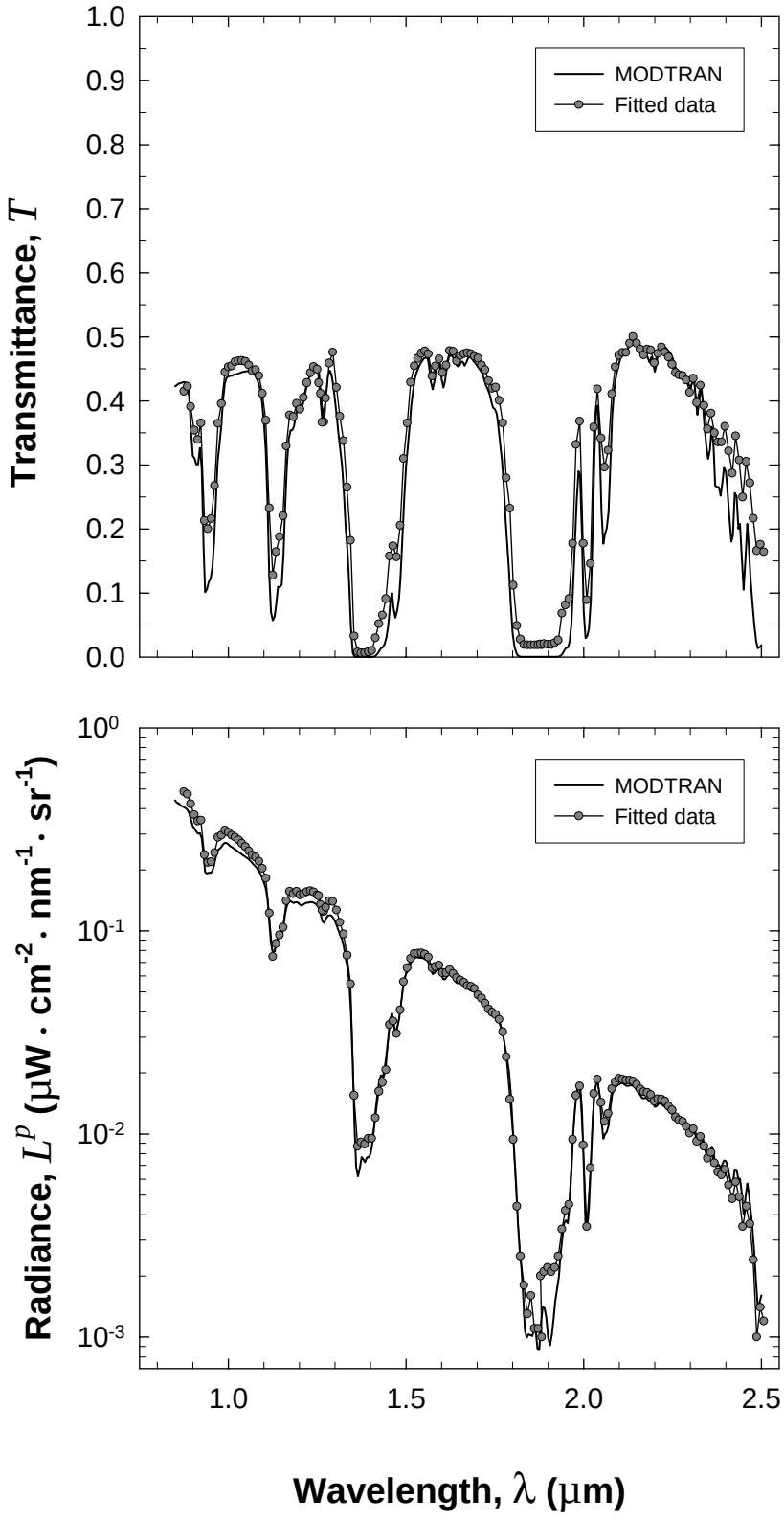

Figure 4. Transmittance and path-scattered radiance derived from fits compared to results from MODTRAN4 with custom aerosol model.

Using these retrieved values, we compute the large-scale wave spectra using Equations 1 and 2 from the data corresponding to Figure 1. We georectify the radiance data, Fourier transform it, and apply a gain factor to compensate for the georectification. The MTF is computed from the retrieved environmental values and divided into the radiance spatial spectra to compute the waveheight spectra. These spectra are integrated to provide a buoy-equivalent (1-dimensional) measurement. These values, computed at 5 wavelengths situated in atmospheric transmission windows, are compared to the western channel buoy measurements in Figure 5. The buoy and image are not collocated, being separated by about 50 km and with a relation that would yield higher waves at the buoy location. Using historical data from both the eastern and western buoys we adjusted the buoy SWH measurement for the location of the images. The adjusted data and the optically derived SWH measurements are shown in Figure 6. The agreement is excellent.

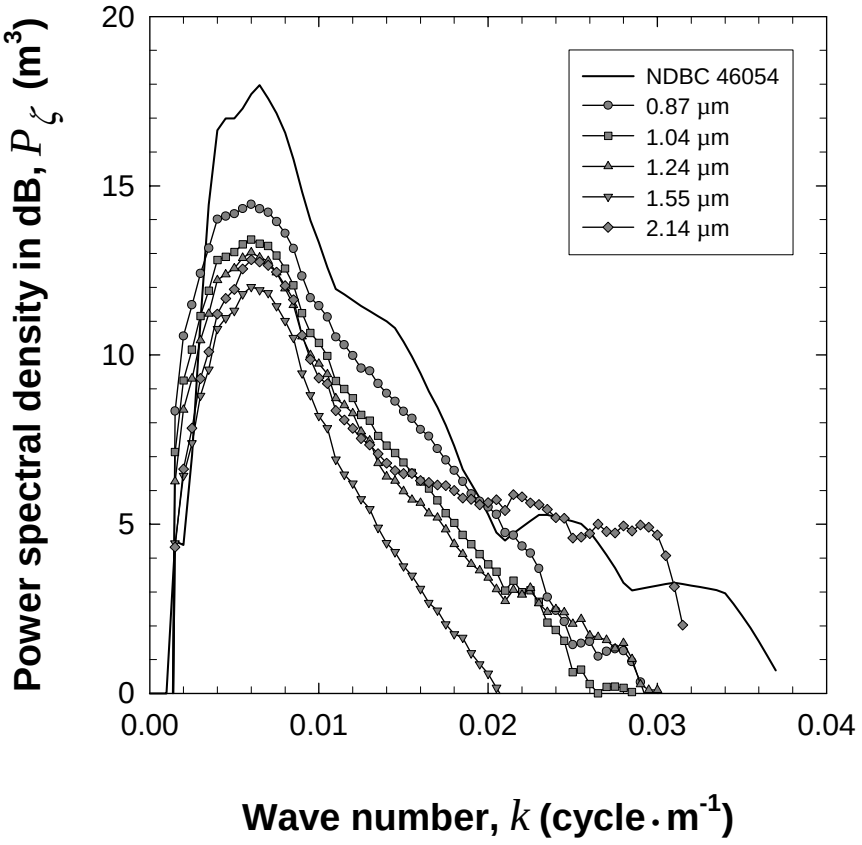

Figure 5. Buoy and optically-derived wave spectra from AVIRIS data acquired on April 10th.

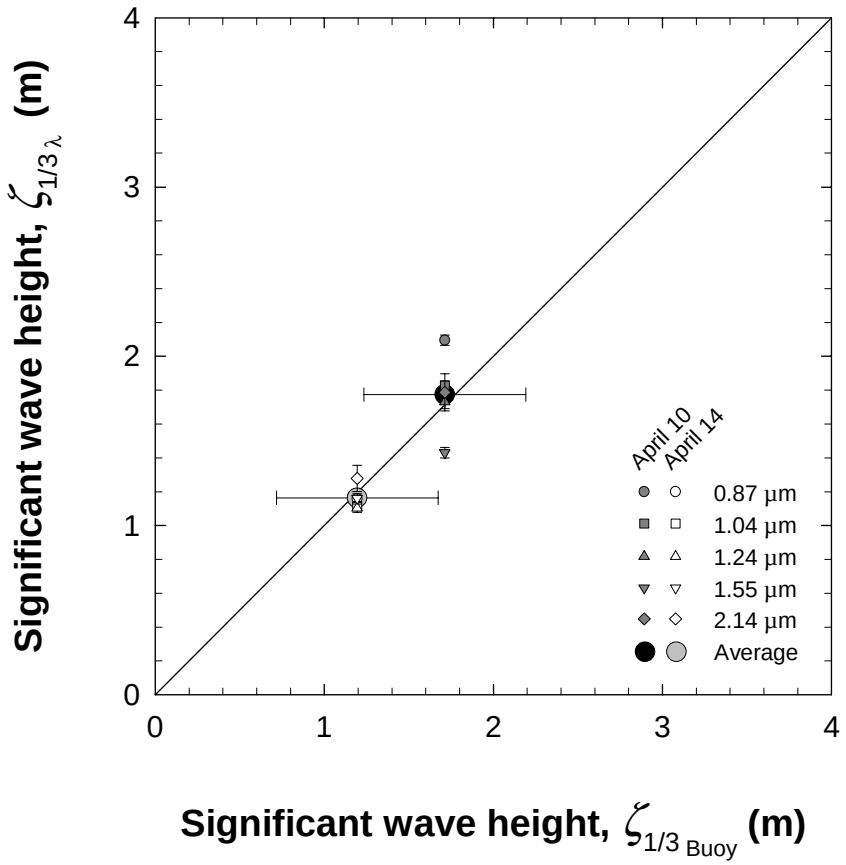

Figure 6. Comparison between optically-derived SWH and buoy measured SWH.

4. INTRINSIC SURFACE REFLECTANCE AND UPWELLING RADIANCE

The most intriguing use of over-ocean hyperspectral data is for the analysis of the water column using the upwelling radiance. To do so, both the atmospheric effects and the surface reflectance must be removed. The atmospheric parameters derived from the fits can be used to remove the effects of the atmosphere in the infrared regime. The aerosol parameters derived from comparisons to MODTRAN simulations provide a means to extrapolate the compensations into the visible regime, though, of course, small aerosol particles that do not influence the infrared wavelengths cannot be accounted for in this manner.

Surface reflectance of direct solar radiation also has been computed using the infrared bands. The physical parameters such as wave slope computed for these data are, of course, electromagnetic wavelength independent. They can be used to remove the effects of glint in the visible regime with the Fresnel reflectivity appropriate for the wavelength.

We have removed atmospheric and solar glinting effects to estimate the upwelling water-column radiance or the remote sensing reflectance. This reflectance can be used to to calculate standard oceanographic products, such as the chlorophyll concentration. Applying standard chlorophyll retrieval algorithms (O'Reilly et al., 1998) to the remote sensing reflectance has produced plausible results. We are refining this technique by including aerosol phase functions and multiple scattering in the computation of the remote sensing reflectance cube.

5. CONCLUSIONS AND SUMMARY

Using several techniques, we have retrieved oceanographic, atmospheric, and water column properties from AVIRIS coastal observations. The oceanographic properties include waveheight spectra and the small-scale wave slope statistics used to infer surface wind speed. Atmospheric properties include atmospheric transmittance, path-scattered radiance and water-vapor column density. The former values are used to infer aerosol loading and extinction characteristics. These parameters are used to compute an intrinsic surface reflectance cube. The glint component can also be removed to provide information on the upwelling water column radiance.

The environmental parameters were obtained using the large field of view of AVIRIS for homogenous atmospheric and oceanic conditions. If the surface-slope parameters are obtained from other sources (e.g., buoy measurements or models), then the atmospheric parameters can be retrieved from Equations 1 and 2. This technique enables a local measurement of atmospheric parameters that may be generally more applicable, especially for spaceborne observations.

6. ACKNOWLEDGEMENTS

This work was funded by the Internal Research and Development Program of XonTech's Special Studies Division. Buoy data were obtained from the National Data Buoy Center's web site and the AVIRIS data were provided by JPL.

7. REFERENCES

Cox, C. and W. Munk, Measurement of the roughness of the sea surface from photographs of the sun's glitter, *J. Opt. Soc. Am., 44*, 838-850, 1954.

Gelpi, C.G., Removing path-scattered radiance from over-ocean spectrometer images for water-vapor estimation, *Remote Sens. Environ., 74*, 414-421, 2000.

Gelpi, C.G., and B. Nguyen, Water-vapor estimation for ocean scenes using modulated surface reflectance, in *Summaries of the Ninth JPL Earth Science Workshop*, edited by R. O. Green, Jet Propulsion Laboratory, Pasadena, California, in press, 2000.

O'Reilly, J.E., S. Maritorena, B.G. Mitchell, D. A. Siegel, K.L. Carder, S.A. Garver, M. Kahru, and C. McClain, Ocean color chlorophyll algorithms for SeaWiFS, *J. Geophys. Res., 103*, No. C11, 24937-24953, 1998.